ORIGINAL ARTICLE

Rational evaluation of the therapeutic effect and dosimetry of auger electrons for radionuclide therapy in a cell culture model

Ayaka Shinohara[1] · Hirofumi Hanaoka[2] · Tetsuya Sakashita[3] · Tatsuhiko Sato[4] · Aiko Yamaguchi[2] · Noriko S. Ishioka[3] · Yoshito Tsushima[5,6]

Abstract

Objective Radionuclide therapy with low-energy auger electron emitters may provide high antitumor efficacy while keeping the toxicity to normal organs low. Here we evaluated the usefulness of an auger electron emitter and compared it with that of a beta emitter for tumor treatment in in vitro models and conducted a dosimetry simulation using radioiodine-labeled metaiodobenzylguanidine (MIBG) as a model compound.

Methods We evaluated the cellular uptake of ^{125}I-MIBG and the therapeutic effects of ^{125}I- and ^{131}I-MIBG in 2D and 3D PC-12 cell culture models. We used a Monte Carlo simulation code (PHITS) to calculate the absorbed radiation dose of ^{125}I or ^{131}I in computer simulation models for 2D and 3D cell cultures. In the dosimetry calculation for the 3D model, several distribution patterns of radionuclide were applied.

Results A higher cumulative dose was observed in the 3D model due to the prolonged retention of MIBG compared to the 2D model. However, ^{125}I-MIBG showed a greater therapeutic effect in the 2D model compared to the 3D model (respective EC_{50} values in the 2D and 3D models: 86.9 and 303.9 MBq/cell), whereas ^{131}I-MIBG showed the opposite result (respective EC_{50} values in the 2D and 3D models: 49.4 and 30.2 MBq/cell). The therapeutic effect of ^{125}I-MIBG was lower than that of ^{131}I-MIBG in both models, but the radionuclide-derived difference was smaller in the 2D model. The dosimetry simulation with PHITS revealed the influence of the radiation quality, the crossfire effect, radionuclide distribution, and tumor shape on the absorbed dose. Application of the heterogeneous distribution series dramatically changed the radiation dose distribution of ^{125}I-MIBG, and mitigated the difference between the estimated and measured therapeutic effects of ^{125}I-MIBG.

Conclusions The therapeutic effect of ^{125}I-MIBG was comparable to that of ^{131}I-MIBG in the 2D model, but the efficacy was inferior to that of ^{131}I-MIBG in the 3D model, since the crossfire effect is negligible and the homogeneous distribution of radionuclides was insufficient. Thus, auger electrons would be suitable for treating small-sized tumors. The design of radiopharmaceuticals with auger electron emitters requires particularly careful consideration of achieving a homogeneous distribution of the compound in the tumor.

Keywords Radionuclide therapy · Auger electron emitter · $^{125/131}$I-Metaiodobenzylguanidine ($^{125/131}$I-MIBG) · 3D cell culture model · Computer simulation

✉ Hirofumi Hanaoka
hanaokah@gunma-u.ac.jp

Extended author information available on the last page of the article

Introduction

Based on the concept of delivering radionuclides selectively to tumor sites while sparing normal tissues from radiation toxicity, radionuclide therapy has been an attractive cancer treatment for decades. The clinical success of radionuclide therapy with β-emitters for certain types of cancer spurred the demand for the expanded application of radionuclide therapy. However, the administration of a sufficiently tumoricidal dose is sometimes restricted due to the maximum tolerant dose limitation. This is partially because of the relatively

low linear energy transfer (LET) (< 0.2 keV/μm) and long path length (1–10 mm in tissue) of β-rays. In particular, when the tumor size is smaller than the path length of β-rays, a substantial amount of the radiation energy escapes from the tumor site and causes normal tissue toxicity [1]. These limitations have led to the consideration of α-emitters as the radionuclides of choice for radionuclide therapy. The higher LET ($- 80$ keV/μm) and shorter path length (50–100 μm) of α-particles compared to β-rays brought about improved therapeutic effects for micrometastases and disseminated tumors [2–4]. However, the widespread application of α-emitters has not been achieved because of these emitters' limited production and availability.

Another potential candidate is low-energy auger electrons. Auger electrons have a tenfold higher LET than β-rays ($- 26$ keV/μm), and their simultaneous action can cause a dense ionization within several cubic nanometers around the point of decay. The dense reactive chemical species produced by auger electrons can cause biological effects similar to those of α-particles [1, 5–7]. In addition, the commercial availability of auger electron emitters, such as ^{123}I, ^{125}I, and ^{111}In, gives auger electrons an additional advantage over α-emitters.

DNA-incorporated, auger electron emitter-labeled deoxyuridine derivatives have indeed demonstrated very high radiotoxicity in vitro [8, 9] and they showed several successful clinical results in patients with cancer (including otherwise incurable metastatic pancreatic cancer in the central nervous system) [10]. Despite these encouraging results, further foundational evaluations are needed for wide acceptance of the use of auger electron emitters for radionuclide therapy in clinical settings.

Previous comparisons of the therapeutic effect of auger electron emitters and β-emitters in in vivo xenograft models have reported conflicting results [1, 11]. Because the therapeutic effect of each radionuclide depends on various factors, especially the tumor size and the intra-tumor distribution of radiopharmaceuticals [12], it would be impractical to attempt to comprehensively evaluate the therapeutic effects of each radiopharmaceutical in every possible condition in in vivo models. Therefore, the influence of the radiation quality and dose on the biological radiotoxicity should be investigated using a more simplified and generalized method. In vitro cell culture models allow us to evaluate the therapeutic effect of each radionuclide under uniform conditions [2, 4, 9, 13]. Moreover, with the use of the obtained dose–response relationship of each radionuclide, computer simulations enable the estimation of the tumor-absorbed dose [14, 15], and thus the therapeutic effect of radionuclide therapy in individual tumors in various conditions.

In this study, we selected radioiodine-labeled metaiodobenzylguanidine (MIBG) as a model compound due to the high availability of its chemically and biologically similar analogs, labeled with either β-emitting ^{131}I or auger electron-emitting ^{125}I, and in light of MIBG's well-defined intracellular localization [16]. We evaluated the therapeutic effects of ^{125}I-MIBG and ^{131}I-MIBG in two-dimensional (2D) and three-dimensional (3D) cell culture models. The 3D cell culture model, also known as a tumor spheroid, well simulates in vivo tumor conditions better than 2D cell culture model, and the 3D cell culture model can thus accommodate the crossfire effect to some extent. We estimated the absorbed radiation dose of each condition using the Monte Carlo code for particle transport simulation (i.e., Particle and Heavy Ion Transport code System, PHITS) which can analyze the transport of almost all radiation particles in 3D matter [17]. Based on the results obtained, we discuss the usefulness and suitable applications of an auger electron emitter for tumor treatment. A new evaluation method to predict the therapeutic effect of radionuclide therapy is also proposed.

Materials and methods

General

Na[125]I (carrier-free, specific activity approx. 650 GBq/mg as iodine) was purchased from American Radiolabeled Chemicals (St. Louis, MO), and Na[131]I (specific activity > 185 GBq/mg as iodine) was purchased from PerkinElmer (Waltham, MA). The reversed-phase high-performance liquid chromatography (RP-HPLC) analysis was performed with a C-18 column (Capcell Pak C18 MGII, 4.6×150 mm, Shiseido, Tokyo) at the flow rate of 1 ml/min eluted with a linear gradient of water containing 0.1% trifluoroacetic acid (TFA) and acetonitrile containing 0.1% TFA from 90:10 to 10:90 in 30 min. All other chemicals used were of the highest purity available. ^{1}H NMR spectra were obtained on an ECA-600 (600 MHz) spectrometer (JEOL, Tokyo), and chemical shifts were identified using NMR predictor software (ChemAxon, Budapest, Hungary). Electrospray ionization mass spectroscopy (ESI-MS) data were obtained with a model LCMS-2020 mass spectrometer (Shimadzu, Kyoto, Japan).

Preparation of [125]I- and ^{131}I-MIBG

The stannyl precursor of radiolabeled MIBG (N,N'-bis(tert-butyloxycarbonyl)-3-(trimethylstannyl) benzylguanidine) was synthesized according to the procedure of Vaidyanathan et al. [18] with some modifications. N,N'-bis(tert-butyloxycarbonyl)-3-iodobenzylguanidine (143.6 mg, 0.30 mmol) in 10 ml of anhydrous toluene was added with $(Ph_3P)_4Pd$ (34.7 mg, 0.03 mmol) and hexamethylditin (412.8 mg, 1.26 mmol) and refluxed under a N_2 atmosphere for 2 h. The reaction mixture was cooled to

room temperature, filtered over a Celite pad, and washed with ethyl acetate. The filtrate was concentrated and purified by column chromatography using a hexane–ethyl acetate gradient to give 37.1 mg (24.2%) of the stannyl precursor as a colorless oil: ^{1}H NMR (CDCl$_3$): 0.27 (s, 9H), 1.35 (s, 9H), 1.49 (s, 9H), 5.16 (s, 2H), 7.20–7.22 (d, 2H), 7.35–36 (d, 1H), 7.42 (s, 1H), 9.31–48 (d, 2H). ESI-MS Calc'd for $C_{21}H_{36}N_3O_4Sn$ (M + H)$^+$: m/z 514.2, found: 514.2.

For the radioiodination, 100 μl of the stannyl precursor (1 mg/ml) dissolved in methanol containing 1% acetic acid was mixed with 2–10 μl of Na$^{125/131}$I solution (^{125}I: 111.0 MBq, ^{131}I: 124.2 MBq) and 5 μl of N-chlorosuccinimide (10 mg/ml) in methanol in a small vial, and the reaction mixture was incubated at room temperature for 10 min. Then, 100 μl of 6 M aqueous HCl was added, and the reaction mixture was incubated at room temperature for 6 h. After the pH of the reaction mixture was neutralized, purification was performed by RP-HPLC, and the solvent was removed in vacuo. The radiochemical purity of MIBGs was determined by RP-HPLC.

In vitro cellular uptake studies

Cellular uptake studies of ^{125}I-MIBG were performed in both a 2D cell culture model and a 3D cell culture model. For the 3D cell culture model, Nunclon Sphera microplates (Thermo Fisher Scientific, Waltham, MA), which support the consistent formation of tumor spheroids, were used. The rat pheochromocytoma cell line PC-12 (American Type Culture Collection ATCC, Manassas, VA) were seeded into 2D and 3D 96-well plates (1.0×10^5 cells/well), then pre-incubated overnight. The disk-shaped tumor spheroids approx. 2 mm in diameter were formed in the 3D plates. Medium-containing ^{125}I-MIBG (5 kBq, 100 μl) was added to each well, and the cells were incubated for 0, 10, 30 min, 1, 3, 6 h, 1, 2, and 3 days at 37 °C. Cells were washed once with phosphate-buffered saline (PBS) and lysed with 0.2 M NaOH. The radioactivity of each cell lysate was measured by a well-type gamma counter (ARC-7001; Hitachi Aloka Medical, Tokyo). In addition, the protein concentration of each well was measured using the Modified Lowry Protein Assay Kit (Thermo Fisher Scientific) according to the manufacturer's protocol.

The uptake of ^{125}I-MIBG was calculated as the percentage of the added activity/mg protein, and the time activity curve was plotted. The cumulative % uptake of radioactivity within the observation period (3 days, % dose/mg protein × day) was calculated by applying a lognormal peak fitting curve model using SigmaPlot ver. 11 (Systat Software, San Jose, CA). The same calculations were performed for ^{131}I-MIBG, taking decay correction into consideration.

In vitro cellular therapeutic studies

For the evaluation of the added radioactivity-dependent cytotoxic effect of ^{125}I-MIBG and ^{131}I-MIBG in vitro, we performed cellular therapeutic studies in the 2D and 3D cell culture models. PC-12 cells were prepared as described above, and then 100 μl of medium-containing ^{125}I-MIBG or ^{131}I-MIBG (0.10, 0.30, 1.0, 3.0, 10, or 30 MBq/ml) was added to each well of 96-well plates, and the plates were incubated for 3 days at 37 °C. After the plates were washed with PBS, the cell viability was measured with a Cell Counting Kit-8 (Dojindo, Kumamoto, Japan) according to the manufacturer's protocol. The results of this assay are presented as the % cell viability relative to non-treated controls. The total effective radioactivity within a single cell (MBq/cell) was calculated using the cumulative % uptake of radioactivity and analyzed by sigmoidal added radioactivity-response fitting using SigmaPlot ver. 11.

Absorbed radiation dose estimation by simulation with PHITS

We estimated the absorbed radiation dose of each model and each radioiodine-labeled MIBG with the use of PHITS, a three-dimensional Monte Carlo particle transport simulation code that simulates various radiation behaviors in substances using nuclear reaction models as well as nuclear and atomic data libraries. PHITS has been used in fields such as engineering, medicine, and science [17, 19]. The accuracy of PHITS for the dosimetry of beta-emitting isotopes was well validated [20].

Briefly, to estimate the absorbed radiation dose per analysis unit (Gy/(Bq/mL)) by PHITS, we defined the simulation areas for 2D and 3D simulation models. The simulation models were designed with Fiji, an open source image-processing distribution of ImageJ (http://imagej.net/Fiji). From the experimentally determined diameter of the PC-12 cells (20 μm), each cell was assumed as a cube 20 μm on a side (volume 8000 μm^3) (Fig. 1a). Using this cube as a standard voxel, the matrix size was determined as $200 \times 200 \times 75$ (4 mm × 4 mm × 1.5 mm). Based on the size of the tumor 3D spheroid (2 mm diameter and 0.5 mm height, Fig. 1b), the 2D tumor area was placed at the center of the bottom of the matrix within a radius of 1 mm (a disk comprised 7,860 cell cubes). Since the height of the tumor spheroid was approx. 0.5 mm, the 3D tumor area was defined as a cylinder comprised 25 layers of the disk (196,500 cell cubes) (Fig. 1a). To take into account the radiation exposure from the radionuclide remaining in the medium, we defined the outside area of each tumor model in the matrix as the culture area.

We next determined the absorbed radiation dose per analysis unit (Gy/(Bq/mL)) in each tumor area for ^{125}I or ^{131}I using PHITS, with the assumption that each radionuclide is
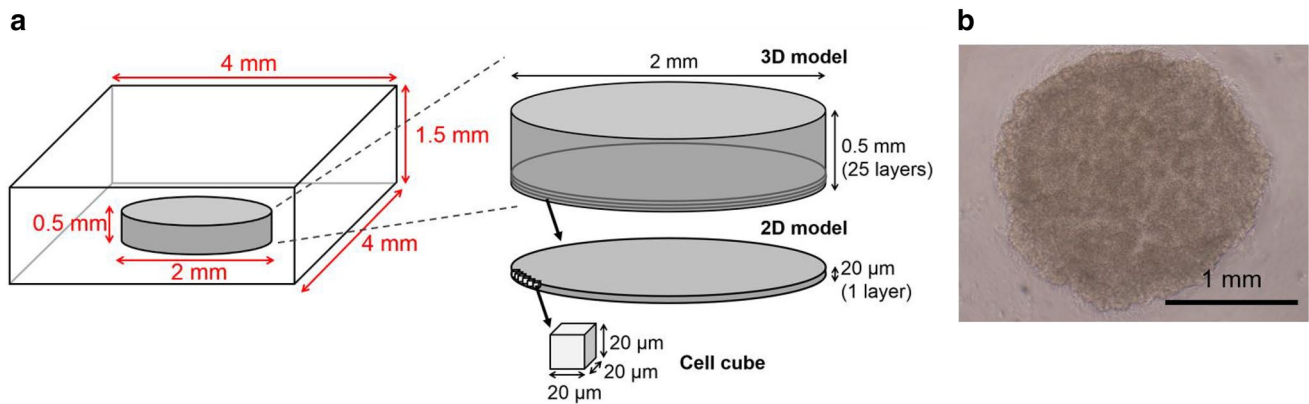
Fig. 1 The cylindrical tumor area and the culture area for the PHITS simulation (**a**) and the spheroid of PC-12 cells (**b**)

distributed either homogeneously or heterogeneously. For the heterogeneous distribution model, it is assumed that MIBG is penetrated from the surface of the spheroid and is not absorbed from the bottom. We created an exponential radioactivity decreasing map with the following equation: $N = N_0 \times \exp(-\ln 2/D_{1/2} \times d)$ (Suppl. Fig. S1). Here, N is the relative radioactivity in each voxel at the depth d, N_0 is the radioactivity at the outer spheroid surface ($= 1$), $D_{1/2}$ is the half-value depth (μm), and d is the depth from the surface (μm). The dose distribution was calculated for $D_{1/2}$ = 10, 30, 50, and 250 μm. The intensity of radioactivity in each cell was normalized according to the predetermined total intensity (196,500). The total intensity was defined by setting the intensity of radioactivity in each cell to 1 in the homogeneous distribution model.

The absorbed radiation dose of tumor from the radionuclide in the tumor and medium was determined individually, and then combined to calculate the total absorbed radiation dose. The concentration of intratumoral radioactivity was calculated based on the results from the abovementioned cellular uptake studies (cumulated radioactivity/cellular volume, Bq/mL). Finally, the absorbed radiation dose (Gy) of each condition was calculated by multiplying these values and the absorbed radiation dose per analysis unit (Gy/(Bq/mL)) in PHITS.

The micro radiation dose from point radiation source of ^{125}I placed at the center of sphere with a radius of 50 μm was also estimated using PHITS. From the obtained estimates, the absorbed radiation dose distribution was plotted against the distance.

Survival estimation of the 3D model by computer simulation

To evaluate the applicability of PHITS for the prediction of the therapeutic effect in the more complicated biological situation, we performed survival estimation studies. To determine the absorbed dose–response relationship, the obtained radiation doses in the 2D simulation model were plotted against the surviving fraction (% cell viability) from the therapeutic studies, and a fitting curve [$SF = \exp(-\ln 2/LD_{50} \times D)$, where SF is the surviving fraction, LD_{50} is the median lethal dose (Gy), and D is the absorbed dose (Gy)] obtained using ORIGIN (MicroCal Software, Northampton, MA). The surviving fractions in the 3D model were then estimated for each radioactivity using the absorbed radiation dose obtained from the 3D simulation models and the formula as described above. We compared these values with the experimental therapeutic results. For the heterogeneous distribution model, we calculated the % cell viability for each cube, and the averaged values of all cubes were determined as the survival fraction.

Statistical analysis

Data are expressed as mean $\pm$ SD. The results were analyzed using the unpaired t test. Differences were considered significant when p values were < 0.05.

Results

In vitro cellular uptake studies

For the initial few hours, the cellular uptake of ^{125}I-MIBG was increased in a time-dependent manner and reached a peak at 6 h in both the 2D and 3D cell culture models (Fig. 2). In the 2D cell culture model, the cellular radioactivity was sharply decreased by 24 h to < 50% of the peak, and it became stable after that. In contrast, the cellular radioactivity in the 3D cell culture model was gradually decreased up to 72 h, and 50% of the radioactivity was finally released. Accordingly, the cumulative % uptake value of the radioactivity of ^{125}I-MIBG and that of
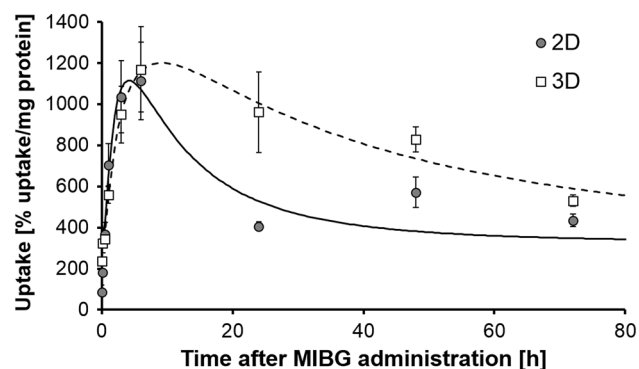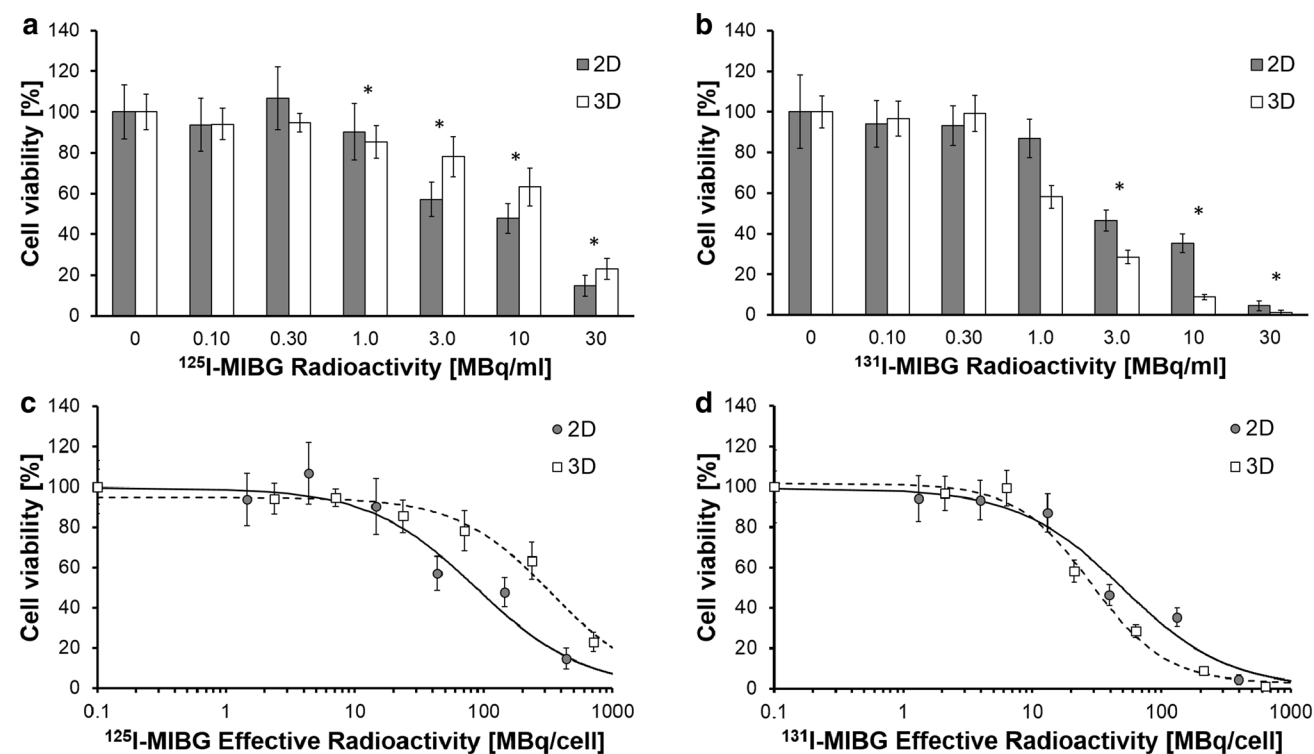
Fig. 2 Time course of the cellular uptake of ^{125}I-MIBG in PC-12 cells in the 2D and 3D culture models. All results are mean ± SD ($n \geq 5$). The fitting curves for the 2D cell culture model (solid line) and 3D cell culture model (dashed line) are shown

^{131}I-MIBG was higher in the 3D culture model (2.58×10^3 and 2.30×10^3 % dose/mg protein × day, respectively) than those in the 2D cell culture model (1.59×10^3 and 1.43×10^3 % dose/mg protein × day, respectively).

In vitro cellular therapeutic study

In our cellular therapeutic studies, we observed radioactivity-dependent cytotoxic effects in each tracer and cell culture model combination, but the effective radioactivity is distinct in each setting. At an added radioactivity > 1.0 MBq/ml, ^{125}I-MIBG reduced the cell viability in the 2D cell culture significantly more than in the 3D cell culture ($p < 0.05$; Fig. 3a). ^{131}I-MIBG showed an inverse effect: the reduction rate of cell viability was significantly greater in the 3D cell culture than that in the 2D cell culture at an added radioactivity > 3.0 MBq/ml ($p < 0.05$; Fig. 3b). We calculated the total effective radioactivity within the cells by multiplying each added radioactivity and the cumulative % uptake, and then plotted these values against the therapeutic effect (Fig. 3c, d).

The opposite therapeutic effect of ^{125}I-MIBG and ^{131}I-MIBG was also observed even after effective radioactivity correction was applied. Based on the sigmoidal fitting curve, the EC$_{50}$ (half-maximal effective concentration) values of ^{125}I-MIBG in the 2D and 3D cell culture models were 86.9 and 303.9 MBq/cell, respectively (Fig. 3c), and those of ^{131}I-MIBG were 49.4 and 30.2 MBq/cell, respectively (Fig. 3d).

Fig. 3 Cell viability of PC-12 cells treated with ^{125}I-MIBG (**a**) or ^{131}I-MIBG (**b**) in the 2D and 3D culture models. All results are mean ± SD ($n \geq 5$). *$p < 0.05$ (2D vs. 3D cell culture model). Cell viability of PC-12 cells treated with ^{125}I-MIBG (**c**) and ^{131}I-MIBG (**d**) for 3 days in the 2D and 3D culture models against the total effective radioactivity within the cells. All results are mean ± SD ($n \geq 5$). The fitting curves for the 2D cell culture model (solid line) and 3D cell culture model (dashed line) are shown

## Absorbed radiation dose estimation by simulation with PHITS

The representative absorbed dose distribution image from the intratumoral ^{125}I/^{131}I-MIBG in the homogeneous and heterogeneous 3D distribution model was shown in Suppl. Fig. S2 and S3, respectively. In the homogeneous distribution model, the calculated averaged absorbed dose per analysis unit of ^{125}I in the 3D simulation model was comparable to that in the 2D simulation model [Suppl. Table S1, 1.96×10^{-12} and 1.89×10^{-12} Gy/(Bq/ml), respectively], whereas the average absorbed dose of ^{131}I in the 3D simulation model was much higher than that in the 2D simulation model [Suppl. Table S1, 23.6×10^{-12} and 12.4×10^{-12} Gy/(Bq/ml), respectively]. In the 3D models, the averaged absorbed dose was also estimated layer by layer. In case of ^{125}I, there was little difference in the averaged absorbed dose between each layer (Suppl. Table S2), $1.88–1.98 \times 10^{-12}$ Gy/(Bq/ml). In contrast, the averaged absorbed dose of ^{131}I showed a gentle gradient from the surface to the center (Suppl. Table S2, 1.22×10^{-11} and 1.81×10^{-11} Gy/(Bq/ml), for the top and middle layers, respectively).

Reflecting the high total effective radioactivity of both MIBGs in the 3D cell culture model compared to that in the 2D cell culture model, the estimated absorbed radiation dose of both ^{125}I-MIBG and ^{131}I-MIBG was higher in the 3D model than those in the 2D model (4.28 vs. 2.49 Gy for ^{125}I-MIBG and 33.45 vs. 5.04 Gy for ^{131}I-MIBG, respectively), on the assumption of 1.0 MBq/ml administration.

The representative absorbed radiation dose distribution image and distance radiation dose plot from point source of the ^{125}I were shown in Suppl. Fig. S4. Absorbed dose from the point source ^{125}I is mainly concentrated within close proximity to the source (less than 0.5 μm in radius), but to a lesser extent, the dose reached up to approximately 10 μm in radius.

Survival estimation of 3D model by computer simulation

The absorbed dose in the 2D simulation model was plotted against the surviving fraction, and fitted by exponential curve (Fig. 4). Note that the surviving fraction is assumed to be radionuclide independent and depends solely on the absorbed dose. When the survival rate for the 3D model was calculated under the assumption of the homogeneous distribution of MIBG in the 3D simulation model, the therapeutic effect of both ^{125}I-MIBG and ^{131}I-MIBG was overestimated (Fig. 5). When the heterogeneous distribution models were applied, the separation of the estimated survival fraction and the experimental results becomes smaller in both the ^{125}I-MIBG and ^{131}I-MIBG models. In case of ^{125}I-MIBG, the estimated survival rate becomes markedly high, and
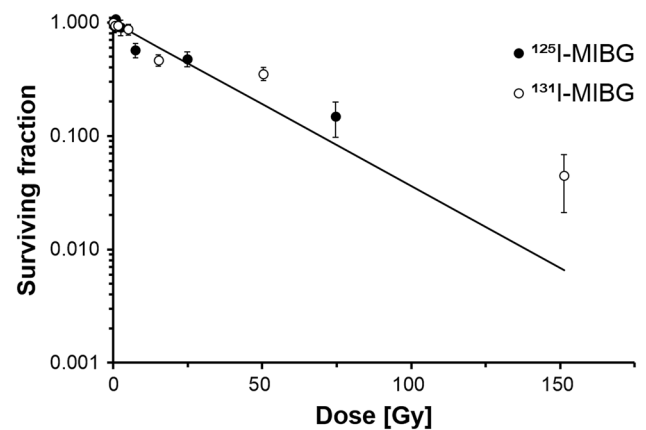

Fig. 4 Surviving fraction of therapeutic studies with the absorbed dose in the 2D model. The solid line is the unified fitting curve for ^{125}I-MIBG and ^{131}I-MIBG

those values in the half-value depth of the 50-μm model were well-matched with the measured results. In the case of ^{131}I-MIBG, the heterogeneous distribution models also mitigate the difference in the survival rate from the measured data, but the separation was not completely eliminated even in the half-value depth of the 10-μm model.

Discussion

In the therapeutic studies of the 2D model, ^{125}I-MIBG showed therapeutic effect comparable to that of ^{131}I-MIBG, even though ^{125}I-MIBG does not reside in the nucleus. Auger electrons can cause cytotoxicity even when the tracers are located in the cytoplasm [21]. The detailed mechanisms of the cytotoxicity remain unknown. Probable factors contributed to the cytotoxicity of ^{125}I-MIBG would be the direct effects such as membrane stress and mitochondrial dysfunction, and to a certain degree, the bystander effect [16]. In addition, micro dose distribution analysis revealed that auger electrons from ^{125}I-MIBG, which is stored in norepinephrine storage granules in the cytoplasm, could occasionally hit the nucleus. The absorbed dose from ^{125}I is distributed up to 10 μm in radius to a lesser extent, though the substantial amount of dose is distributed within a radius of 0.5 μm. These results provide the rationale for the use of ^{125}I-MIBG to evaluate the usefulness and application of auger electrons.

Since the crossfire effect by auger electrons is negligible, it can be assumed that the therapeutic effect of ^{125}I-MIBG is solely dependent on the cumulative radioactivity. The cumulative % uptake of radioactivity in the 3D model was higher than that in the 2D model due to the difference in the release pattern of MIBG. The release pattern of the cellular radioactivity in the 2D model was steep, whereas that in the 3D model was gradual. This difference would be attributable
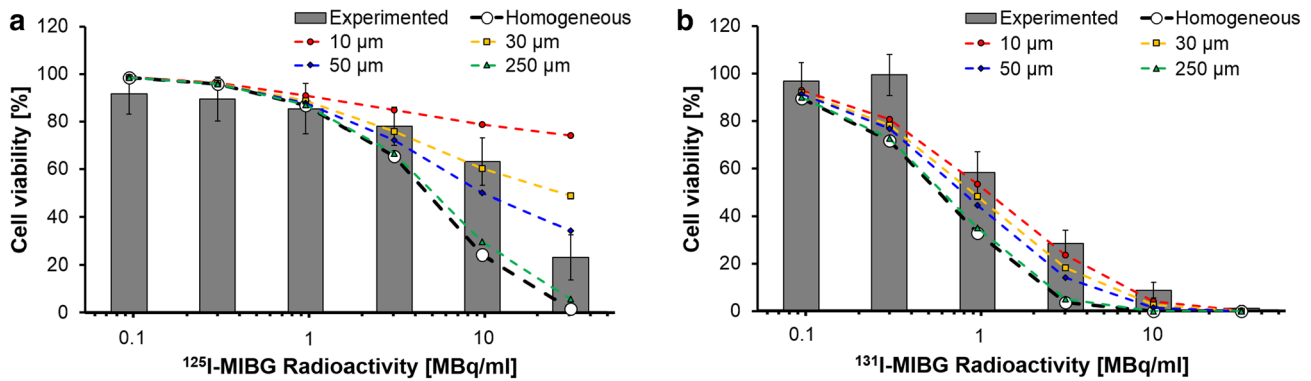
Fig. 5 Estimation of the cell viability of PC-12 cells in the 3D model treated with ^{125}I-MIBG (**a**) or ^{131}I-MIBG (**b**). Gray bars are the experimental results in the 3D cell culture model using the same data as in Fig. 3. White circles are the estimated survival rate data under the assumption of a homogeneous distribution of MIBG. The other markers are the estimated survival rate data under the assumption of a heterogeneous distribution of MIBG with various half-value depths (µm)

to the density of the cells; the higher cellular density in the 3D model relative to the 2D model makes it easier for the surrounding cells to reuptake MIBG more frequently. However, ^{125}I-MIBG showed a greater therapeutic effect in the 2D model than that in the 3D model even after the effective radioactivity was corrected using the cumulative % uptake. Since the compounds' penetration in the 3D spheroid is limited [22, 23], the level of radiation exposure was too weak to cause a cytocidal effect in the inner part of the spheroid where the concentration of ^{125}I-MIBG was low. In contrast, despite the heterogeneous distribution in the 3D spheroid, ^{131}I-MIBG showed higher therapeutic effect in the 3D model than that in the 2D model due to the crossfire effect [11]. These results indicate that the design of radiopharmaceuticals with auger electron emitters requires particularly careful consideration to achieve the homogeneous distribution of the compound in the tumor, compared to β-emitters or α-emitters.

Assuming a homogeneous distribution of MIBG, the PHITS simulation well reflected the difference in the radiation quality and the crossfire effect between β-ray and auger electrons (Suppl. Fig. S2). In both the 2D and 3D models, ^{125}I-MIBG showed a comparable average absorbed dose. In contrast, ^{131}I-MIBG showed a much higher average absorbed dose in the 3D model compared to that in the 2D model, and the average absorbed doses of ^{131}I-MIBG increased gradually from the surface layer to the middle layers. However, there was a discrepancy between the measured and estimated values when the therapeutic effect of MIBG in the 3D model was estimated based on the homogeneous distribution model. We therefore also calculated the simulation models under the assumption of the heterogeneous distribution. Using PHITS, we can set a micro-distribution of the radiation source and calculate an absorbed dose at an arbitrary point. The heterogeneous distribution series

of ^{125}I-MIBG dramatically changed the distribution of the radiation dose (Suppl. Fig. S3), and the discrepancy between the measured and estimated values became smaller. These results strongly suggested the existence of distribution heterogeneity of MIBG in the spheroids, thus reinforcing the requirement for radiopharmaceuticals used with auger electron emitters to be distributed homogeneously in the tumor for radionuclide therapy.

However, in the case of ^{131}I-MIBG, the heterogeneous distribution series still overestimated the therapeutic effect, probably due to the suboptimal curve fitting. In general, the surviving fraction of cells irradiated by external radiation dose D can be expressed by an exponential fitting curve, $\exp(-\alpha D - \beta D^2)$ with positive α and β coefficients. The application of the fitting model to our data results in an overestimation of the surviving fraction, especially at higher radioactivity. Thus, the establishment of the optimal formula for estimating the survival fraction of the radionuclide therapy needs further investigation.

Considering the clinical situation, a consensus regarding the absorbed dose–response relationship for radionuclide therapy has not yet been reached, even with the accumulated clinical evidence of external radiation therapy. This is presumably not only because of the insufficiency of the number of case series of radionuclide therapy but also due to the immaturity of the technique for accurately assessing the radiopharmaceutical-derived absorbed radiation doses. Simulation with PHITS enables the estimation of radiation dose distributions of any given tumor for which biodistribution data of the respective radiopharmaceutical are available, and this will eventually contribute to the establishment of robust absorbed dose–response relationships for radionuclide therapy. This approach may also permit the patient-based selection of the suitable radionuclide and radiopharmaceuticals for individual tumors.

The advantage of β-emitters over auger electron emitters increases with an increase in the size of the tumor. In our present in vitro studies, the therapeutic effect of ^{125}I-MIBG was lower than that of ^{131}I-MIBG in both the 2D and 3D models, though the radionuclide-derived difference was smaller in the 2D model. In the simulation study by Wolfgang et al. [24], the therapeutic effects of ^{125}I-MIBG and ^{131}I-MIBG on tumor spheroids were equal for tumors up to approx. 100 μm in diameter. The therapeutic effect of an auger electron emitter can be enhanced using radiopharmaceuticals that accumulate in the nucleus [5–7]. From these factors, we can deduce that auger electrons are suitable for treating tumors with a small size such as micro-metastases and disseminated small tumors rather than the tumors of a certain size. In addition, our PHITS simulation clearly demonstrated that the radiation exposure from ^{125}I was restricted specifically in the tumor lesion, whereas that from ^{131}I extended widely to the surrounding area. These results indicating the expectedly very low side effect of auger electron may enable higher radiation dose administration to the patients. Radionuclide therapy with auger electrons has the potential to provide a better therapeutic effect than that with β-emitters in the case of small tumors.

There were several limitations in this study. Although the difference in the therapeutic effect between auger electrons and β-rays was clearly demonstrated in our spheroid model, the size of the spheroid might affect the distribution patterns of radiopharmaceuticals and the degree of crossfire effect. To simplify the simulation models, the shapes of the cells and the spheroid were deformed, but even under these assumptions, the estimated results agreed well with the experimental results. We will be able to obtain more precise results using more accurate models. We did not perform in vitro experiments multiple times in the exact same condition, due to the usage limitation of radionuclide in our facility. But similar tendencies were observed in the preliminary experiments. Besides, all in vitro therapeutic studies were performed at the same time and in the same condition. Taken together, these factors support the reproducibility of our results and validate the usefulness of auger electrons.

In conclusion, ^{125}I-MIBG showed a therapeutic effect in both 2D and 3D cell culture models, but its therapeutic efficacy was lower than that of ^{131}I-MIBG, especially in the 3D model. Thus, radiation therapy with auger electrons would be suitable for small-sized tumors such as small metastases. In addition, the design of radiopharmaceuticals with auger electron emitters requires the very careful consideration of how to achieve a homogeneous distribution of the compound in the tumor. In the present study, the simulation with PHITS estimated the absorbed radiation dose of ^{125}I-MIBG, and the obtained dose–response relationship provided an accurate prediction of the therapeutic effect of ^{125}I-MIBG in the 3D spheroid. This approach may thus enable the evaluation of the radiation dose for any given tumor for which the distribution of the respective radiopharmaceutical is available.

Compliance with ethical standards

References

1. Behr TM, Béhé M, Löhr M, Sgouros G, Angerstein C, Wehrmann E, et al. Therapeutic advantages of Auger electron-over beta-emitting radiometals or radioiodine when conjugated to internalizing antibodies. Eur J Nucl Med. 2000;27:753–65.

2. Andersson H, Elgqvist J, Horvath G, Hultborn R, Jacobsson L, Jensen H, et al. Astatine-211-labeled antibodies for treatment of disseminated ovarian cancer: an overview of results in an ovarian tumor model. Clin Cancer Res. 2003;9:3914–21.

3. Teiluf K, Seidl C, Blechert B, Gaertner FC, Gilbertz KP, Fernandez V, et al. α-Radioimmunotherapy with ^{213}Bi-anti-CD38 immunoconjugates is effective in a mouse model of human multiple myeloma. Oncotarget. 2015;6:4692–703.

4. Hagemann UB, Wickstroem K, Wang E, Shea AO, Sponheim K, Karlsson J, et al. In vitro and in vivo efficacy of a novel CD33-targeted thorium-227 conjugate for the treatment of acute myeloid leukemia. Mol Cancer Ther. 2016;15:2422–31.

5. Kassis AI. The amazing world of auger electrons. Int J Radiat Biol. 2004;80:789–803.

6. Kassis AI. Molecular and cellular radiobiological effects of Auger emitting radionuclides. Radiat Prot Dosimetry. 2011;143:241–7.

7. Sastry KS. Biological effects of the Auger emitter iodine-125: a review. Report No. 1 of AAPM Nuclear Medicine Task Group No. 6. Med Phys. 1992;19:1361–70.

8. Kassis AI, Sastry KS, Adelstein SJ. Kinetics of uptake, retention, and radiotoxicity of ^{125}IUdR in mammalian cells: Implications of localized energy deposition by Auger processes. Radiat Res. 1987;109:78–89.

9. Kassis AI, Adelstein SJ, Haydock C, Sastry KS, McElvany KD, Welch MJ. Lethality of Auger electrons from the decay of bromine-77 in the DNA of mammalian cells. Radiat Res. 1982;90:362–73.

10. Rebischung C, Hoffmann D, Stefani L, Desruet MD, Wang K, Adelstein SJ, et al. First human treatment of resistant neoplastic meningitis by intrathecal administration of MTX plus ^{125}IUdR. Int J Radiat Biol. 2008;84:1123–9.

11. Rutgers M, Buitenhuis CK, van der Valk MA, Hoefnagel CA, Voûte PA, Smets LA. [^{131}I] and [^{125}I] metaiodobenzylguanidine therapy in macroscopic and microscopic tumors: a comparative study in SK-N-SH human neuroblastoma and PC12 rat pheochromocytoma xenografts. Int J Cancer. 2000;90:312–25.

12. Brans B, Bodei L, Giammarile F, Linden O, Luster M, Oyen WJ, et al. Clinical radionuclide therapy dosimetry: the quest for the "Holy Gray". Eur J Nucl Med Mol Imaging. 2007;34:772–86.

13. Govindan SV, Goldenberg DM, Elsamra SE, Griffiths GL, Ong GL, Brechbiel MW, et al. Radionuclides linked to a CD74 antibody as therapeutic agents for B-cell lymphoma: comparison of Auger electron emitters with beta-particle emitters. J Nucl Med. 2000;41:2089–97.

14. Bousis C, Emfietzoglou D, Hadjidoukas P, Nikjoo H. Monte Carlo single-cell dosimetry of auger-electron emitting radionuclides. Phys Med Biol. 2010;55:2555–72.

15. Bousis C, Emfietzoglou D, Nikjoo H. Monte Carlo single-cell dosimetry of I-131, I-125 and I-123 for targeted

radioimmunotherapy of B-cell lymphoma. Int J Radiat Biol. 2012;88:908–15.

16. Boyd M, Ross SC, Dorrens J, Fullerton NE, Tan KW, Zalutsky MR, et al. Radiation-induced biologic bystander effect elicited in vitro by targeted radiopharmaceuticals labeled with α-, β-, and auger electron-emitting radionuclides. J Nucl Med. 2006;47:1007–15.

17. Sato T, Niita K, Matsuda N, Hashimoto S, Iwamoto Y, Noda S, et al. Particle and heavy ion transport code system PHITS, version 2.52. J Nucl Sci Technol. 2013;50:9,913–23.

18. Vaidyanathan G, Affleck DJ, Alston KL, Zalutsky MR. A tin precursor for the synthesis of no-carrier-added [*I]MIBG and [^{211}At]MABG. J Label Compd Radiopharm. 2007;50:177–82.

19. Sato T, Niita K, Matsuda N, Hashimoto S, Iwamoto Y, Noda S, et al. Overview of the PHITS code and its application to medical physics. Prog Nucl Sci Technol. 2014;4:879–82.

20. Shiiba T, Kuga N, Kuroiwa Y, Sato T. Evaluation of the accuracy of mono-energetic electron and beta-emitting isotope dose-point kernels using particle and heavy ion transport code system: PHITS. App Radiat Isot. 2017;128:199–203.

21. Pouget JP, Santoro L, Raymond L, Chouin N, Bardiès M, Bascoul-Mollevi C, et al. Cell membrane is a more sensitive target than cytoplasm to dense ionization produced by auger electrons. Radiat Res. 2008;170:192–200.

22. Sagnella SM, Duong H, MacMillan A, Boyer C, Whan R, McCarroll JA, et al. Dextran-based doxorubicin nanocarriers with improved tumor penetration. Biomacromol. 2014;15:262–75.

23. Groh CM, Hubbard ME, Jones PF, Loadman PM, Periasamy N, Sleeman BD, et al. Mathematical and computational models of drug transport in tumours. J R Soc Interface. 2014;11:20131173.

24. Weber W, Weber J, Senekowitsch-Schmidtke R. Therapeutic effect of m-[^{131}I]- and m-[^{125}I]iodobenzylguanidine on neuroblastoma multicellular tumor spheroids of different sizes. Cancer Res. 1996;56:5428–34.

Affiliations

Ayaka Shinohara[1] · Hirofumi Hanaoka[2] · Tetsuya Sakashita[3] · Tatsuhiko Sato[4] · Aiko Yamaguchi[2] · Noriko S. Ishioka[3] · Yoshito Tsushima[5,6]

[1] Department of Heavy Ion Beam Medical Physics and Biology, Gunma University Graduate School of Medicine, 3-39-22 Showa, Maebashi 371-8511, Japan

[2] Department of Bioimaging Information Analysis, Gunma University Graduate School of Medicine, 3-39-22 Showa, Maebashi 371-8511, Japan

[3] Quantum Beam Science Research Directorate, National Institutes for Quantum and Radiological Science and Technology, 1233 Watanuki-machi, Takasaki 370-1292, Japan

[4] Nuclear Science and Engineering Center, Japan Atomic Energy Agency, 2-4 Shirakata, Tokai 319-1195, Japan

[5] Department of Diagnostic Radiology and Nuclear Medicine, Gunma University Graduate School of Medicine, 3-39-22 Showa, Maebashi 371-8511, Japan

[6] Research Program for Diagnostic and Molecular Imaging, Division of Integrated Oncology Research, Gunma University Initiative for Advanced Research (GIAR), Gunma University Graduate School of Medicine, 3-39-22 Showa, Maebashi 371-8511, Japan

Rational evaluation of the therapeutic effect and dosimetry of auger electrons for radionuclide therapy in a cell culture model

Annals of Nuclear Medicine

Ayaka Shinohara, Hirofumi Hanaoka[*], Tetsuya Sakashita, Tatsuhiko Sato, Aiko Yamaguchi, Noriko S. Ishioka, Yoshito Tsushima

***Corresponding author:** Dr. Hirofumi Hanaoka, Department of Bioimaging Information Analysis, Gunma University Graduate School of Medicine, 3-39-22 Showa, Maebashi 371-8511, Japan. Tel.: +81-27-220-8403; Fax: +81-27-220-8409. E-mail: hanaokah@gunma-u.ac.jp
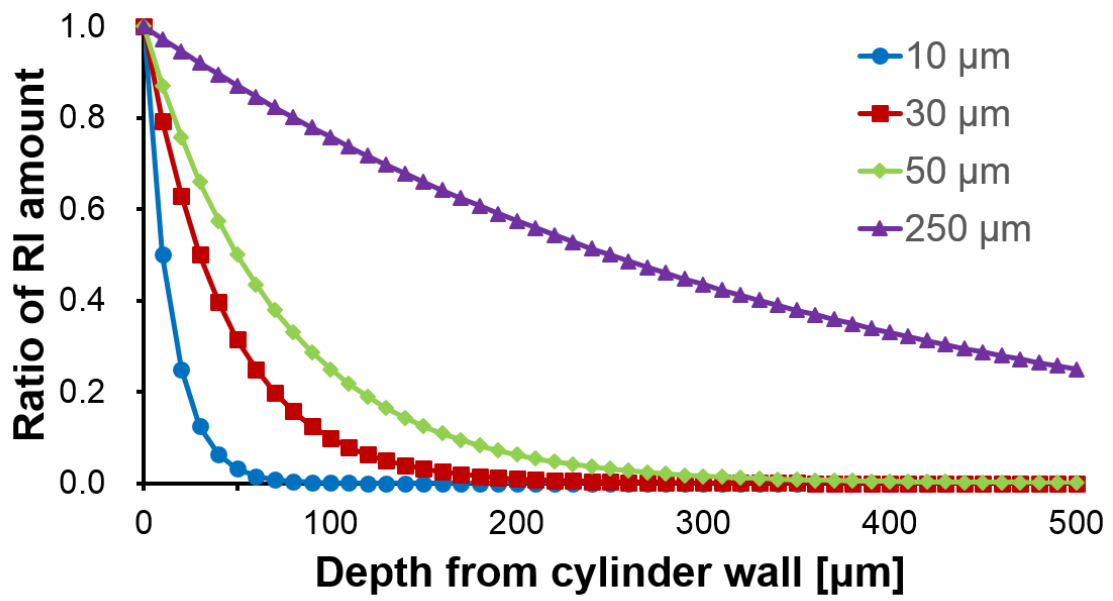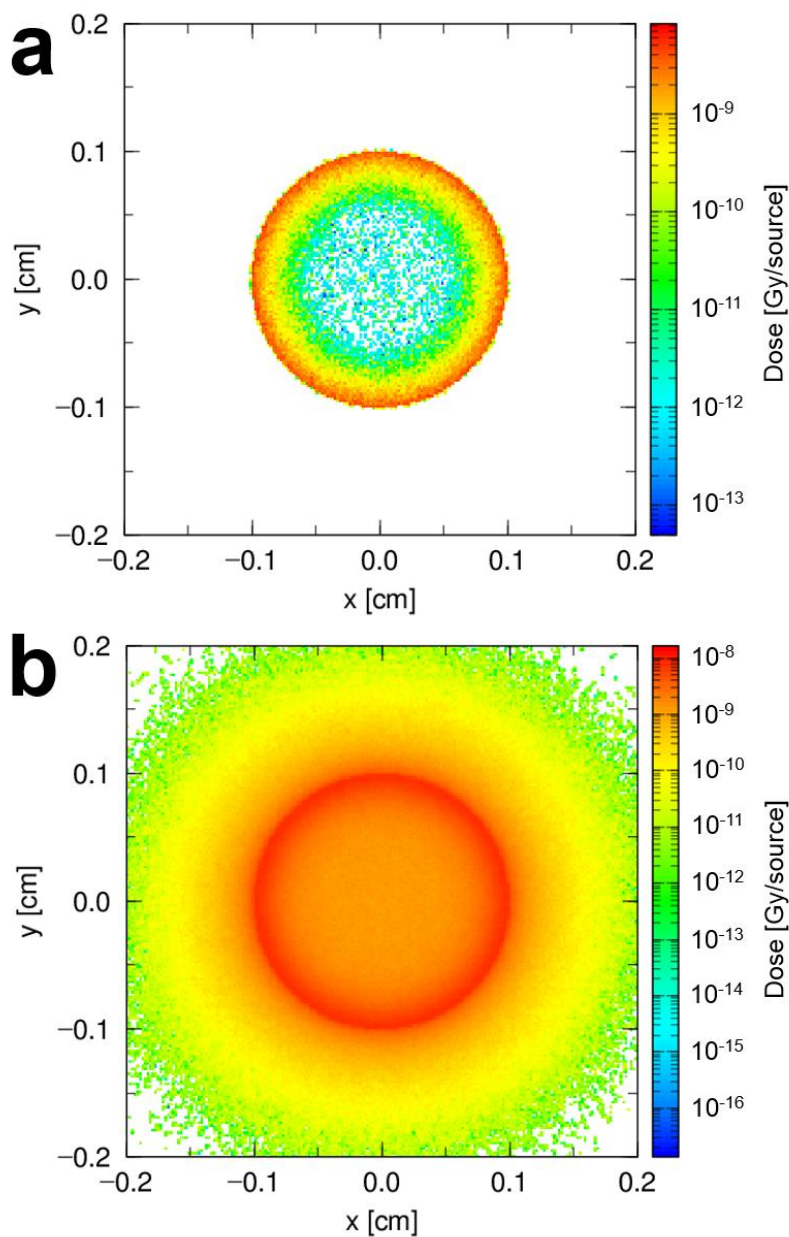
Suppl. Fig. S1. Radioactivity decreasing curve with depth from surface for $D_{1/2}$ = 10, 30, 50, and 250 µm.
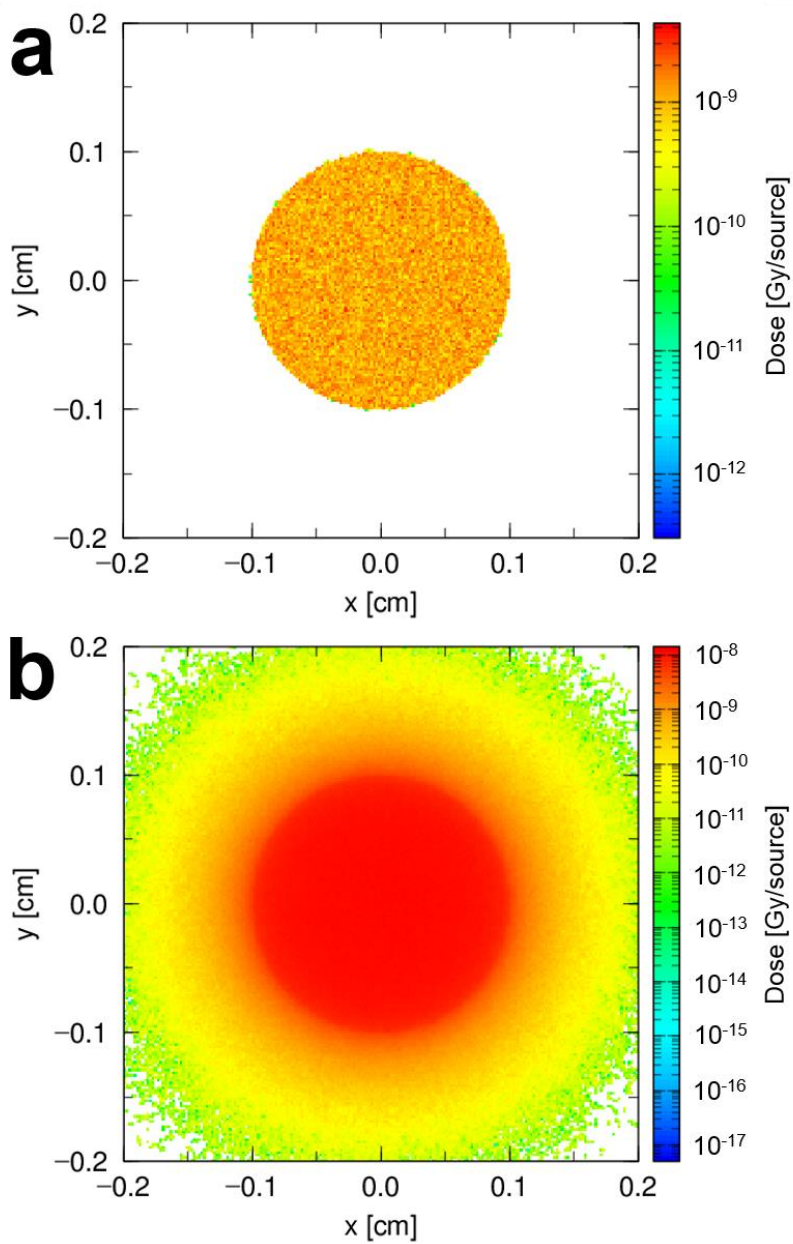
Suppl. Fig. S2. The representative absorbed dose distribution image from the intratumoral ^{125}I-MIBG (**a**) or ^{131}I-MIBG (**b**) in the homogeneous distribution 3D model (the 12th layer). Data are normalized to 1 electron emission.

Suppl. Fig. S3. The representative absorbed radiation dose distribution image from the intratumoral ^{125}I-MIBG (**a**) or ^{131}I-MIBG (**b**) in the heterogeneous distribution 3D model ($D_{1/2}$=50 μm, the 25th layer). The dose from ^{125}I-MIBG is high at the surface, but it is attenuated at the central part. The dose from ^{131}I-MIBG is high even in the central part. Data are normalized to 1 electron emission.

Suppl. Table S1. The absorbed radiation dose of ^{125}I-MIBG and ^{131}I-MIBG from the radionuclide in the tumor area, culture area, and their sum in the homogeneous distribution model

| Model	Absorbed dose [Gy/(Bq/ml)]		
	Tumor area	Culture area	Total
^{125}I-MIBG (2D)	1.83×10^{-12}	0.0625×10^{-12}	1.89×10^{-12}
^{125}I-MIBG (3D)	1.95×10^{-12}	0.00528×10^{-12}	1.96×10^{-12}
^{131}I-MIBG (2D)	2.20×10^{-12}	10.2×10^{-12}	12.4×10^{-12}
^{131}I-MIBG (3D)	16.1×10^{-12}	7.55×10^{-12}	23.6×10^{-12}

The statistical uncertainties of these data are less than a few percent on average, except for 17.5% of ^{125}I-MIBG medium. However, the contribution of ^{125}I-MIBG medium to the total absorbed dose is <1%.

Suppl. Table S2. The calculated average absorbed dose of each layer in the homogeneous distribution model

Layer	Dose [Gy/(Bq/ml)]	
	^{125}I-MIBG	^{131}I-MIBG
1	1.88×10^{-12}	1.22×10^{-11}
2	1.95×10^{-12}	1.38×10^{-11}
3	1.96×10^{-12}	1.48×10^{-11}
4	1.95×10^{-12}	1.56×10^{-11}
5	1.97×10^{-12}	1.63×10^{-11}
6	1.94×10^{-12}	1.67×10^{-11}
7	1.95×10^{-12}	1.71×10^{-11}
8	1.96×10^{-12}	1.75×10^{-11}
9	1.96×10^{-12}	1.77×10^{-11}
10	1.95×10^{-12}	1.79×10^{-11}
11	1.95×10^{-12}	1.80×10^{-11}
12	1.98×10^{-12}	1.81×10^{-11}
13	1.97×10^{-12}	1.81×10^{-11}
14	1.96×10^{-12}	1.80×10^{-11}
15	1.96×10^{-12}	1.79×10^{-11}
16	1.96×10^{-12}	1.78×10^{-11}
17	1.95×10^{-12}	1.75×10^{-11}
18	1.93×10^{-12}	1.72×10^{-11}
19	1.97×10^{-12}	1.68×10^{-11}
20	1.96×10^{-12}	1.63×10^{-11}
21	1.96×10^{-12}	1.58×10^{-11}
22	1.96×10^{-12}	1.49×10^{-11}
23	1.96×10^{-12}	1.39×10^{-11}
24	1.96×10^{-12}	1.24×10^{-11}
25	1.90×10^{-12}	9.86×10^{-12}

The dose of each layer from ^{125}I-MIBG was comparable, whereas that from ^{131}I-MIBG gradually increased from the top or bottom layer and reached its peak at the middle layer. The statistical uncertainties of these data for ^{125}I-MIBG and ^{131}I-MIBG are 0.41% and 0.16% on average, respectively.
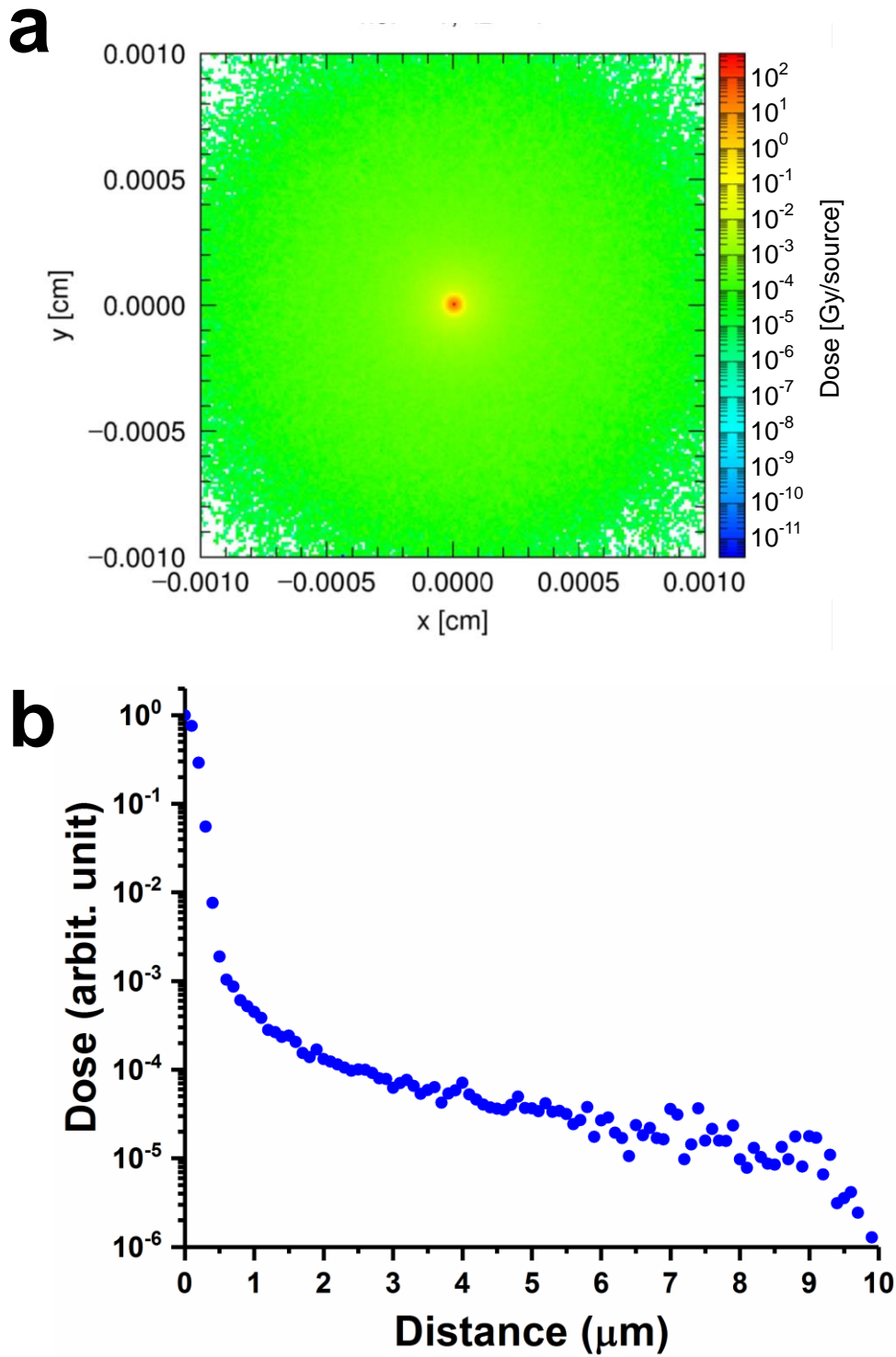
Suppl. Fig. S4. The representative absorbed radiation dose distribution image (**a**) and distance-radiation dose plot (**b**) from the point source of ^{125}I at the center position (20 μm square slice at middle part of the sphere).